World Conference on Timber Engineering Oslo 2023

PYTHON-BASED PLATE MODEL TO SIMULATE THE EFFECT OF KNOTTY AREAS ON SAWN TIMBER.

Jorge Uribe Cisternas[1], Diego Valdivieso Cascante[2]

ABSTRACT: This paper introduces a computational python-based model of a timber plate of Pinus Radiata D. Don specie grown in Chile. The effect of knotty areas is considered for the simulation of stiffness and resistance in a simply supported plate subjected to out-of-plane bending assessing the failure with the Von Mises normalized and Tsai-Wu criteria. The computational model is implemented based on the Reissner-Mindlin plate theory, considering a rectangular orthotropic model to simulate the behavior of wood. When the knotty area ratio (KAR) reaches its maximal value, 1, stiffness and resistance decrease by 19% and 56%, respectively. Through the Monte-Carlo method, 500 wooden plates are simulated by randomly distributing the lengths of internodes and whorls, which shows a difference of 14% in vertical displacement. It is concluded that the open-source numerical model was able to capture the effect of the knotty areas on the bending behavior of timber elements. The next step involves the calibration of the input parameters of the numerical model from the test results.

KEYWORDS: Plate, KAR, Whorl, Internode, Finite Elements Models, Pinus Radiata

1 INTRODUCTION

Wood has been used repeatedly in Chile for small constructions. Nowadays, the need to carry out sustainable constructions based on renewable materials and with that cause a low impact on the environment makes wood head the list of most required materials in the future.

For the same reason, the Chilean construction industry has evaluated the alternative of building wooden constructions to eventually replace concrete and steel constructions. However, compared to concrete and steel, there is still a lack of knowledge about the behavior of wood products made from Pinus radiata grown in Chile and the effect of their natural defects (i.e., knotty area and its distribution on the tree length) on their mechanical properties [1].

This article aims to contribute to the development of an open-source plate model based on Python that allows quantifying the effects of knotty areas on the bending behavior of wood elements through the finite element method.

2 COMPUTATIONAL MODEL

2.1 GENERAL

A plate is defined as a flat solid whose thickness is much smaller than its other dimensions (length and width). In this paper, a finite element model for plate bending is presented based on the Reissner-Mindlin plate theory for small elastic strains, which includes the transverse shear effect [2,15] (see Figure 1).

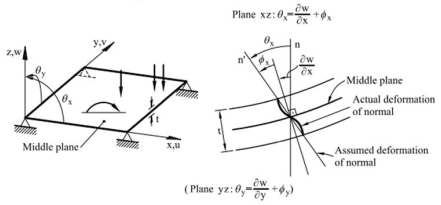

Figure 1: *Reissner-Mindlin plate theory. Sign convention for the displacements and the rotations of the normal. Taken from [9].*

2.2 FORMULATION

2.2.1 Force Formulation

According to [5], the strong formulation of the boundary problem of plate theory is:

$$
(S)\quad \left\{ \begin{array}{l} \textit{Considering } F, C_\alpha, M_\alpha, Q, W \textit{ and } \Theta_\alpha, \textit{find } w \textit{ and } \theta_\alpha \textit{ such that:} \\ \left.\begin{array}{rl} m_{\alpha\beta,\beta} - q_\alpha + C_\alpha &= 0 \\ q_{\alpha,\alpha} + F &= 0 \\ m_{\alpha\beta} &= -c_{\alpha\beta\gamma\delta} k_{\gamma\delta} \\ q_\alpha &= c_{\alpha\beta}\gamma_\beta \\ k_{\alpha\beta} &= \theta_{(\alpha,\beta)} \\ \gamma_\alpha &= -\theta_\alpha + w_{,\alpha} \end{array}\right\} \forall x \in A \\ \left.\begin{array}{rl} \theta_\alpha &= \Theta_\alpha \\ w &= W \\ m_{\alpha n} = m_{\alpha\beta} n_\beta &= \mathrm{M}_\alpha \end{array}\right\} \begin{array}{l} \forall x \in \Gamma_{\theta\alpha} \\ \forall x \in \Gamma_w \\ \forall x \in \Gamma_M \end{array} \end{array} \right.
$$

[1]Jorge Uribe Cisternas, Universidad Nacional Andrés Bello, Chile, j.uribecisternas@uandresbello.edu
[2] Diego Valdivieso, Pontificia Universidad Católica de Chile, Centro Nacional de Excelencia para la Industria de la Madera (CENAMAD) & Centro de Innovación en Madera (CIM UC-CORMA, Chile, dnvaldivieso@uc.cl. University of Colorado at Boulder, USA, diego.valdivieso@colorado.edu

https://doi.org/10.52202/069179-0052

$$q_n = q_\alpha n_\alpha = Q \qquad \} \forall x \in \Gamma_Q$$

Where, F= applied transverse force per unit area, C_α= applied moment couple per unit area, M_α= prescribed moments at the boundary, Q= prescribed shear force at the boundary, W= prescribed displacement at the border. Also $m_{\alpha\beta}$ is the moment tensor, q_α is the shear force vector $k_{\alpha\beta}$ is the curvature tensor and γ_α is the shear strain vector. The $\Gamma'_{(.)S}$ represents the different parts of the boundary.

2.2.2 Finite Element Formulation

We start the weak formulation by defining the spaces:

$$\mathcal{S} = \{w, \theta_1, \theta_2 \in H^1(\Omega, \mathbb{R}) | w = W \ \forall \in \Gamma_w, \theta_\alpha = \Theta_\alpha \ \forall x \in \Gamma_{\theta\alpha}\}$$

$$\mathcal{V}_{\theta\alpha} = \{\delta\theta_\alpha \in H^1(\Omega, \mathbb{R}) | \delta\theta_\alpha = 0, \ \forall x \in \Gamma_{\theta\alpha}\}$$

$$\mathcal{V}_w = \{\delta w \in H^1(\Omega, \mathbb{R}) | \delta w = 0, \ \forall x \in \Gamma_w\}$$

Where $\mathcal{S}$ is the solution space, $\mathcal{V}_{\theta\alpha}$ and $\mathcal{V}_w$ are the test spaces, H^1 is the Sobolev space, W and Ω_α are the prescribed displacements and rotations (essential or Dirichlet conditions), and $\Gamma_{\theta\alpha}$ and Γ_w are the Dirichlet boundaries.

The variational formulation is obtained by multiplying the equations of the strong formulation by the functions test and integrated by parts in the domain $w = A$. Defining $\delta\gamma_\alpha = \delta\theta_\alpha + \delta_{w,\alpha}$ we have:

$$(W)\begin{cases} Considering\ F, C_\alpha, M_\alpha, Q, W\ and\ \Theta_\alpha, find\ w\ and \\ \theta_\alpha \in \mathcal{V}\ such\ that, \forall \delta_w \in \mathcal{V}\ and\ \delta\theta_\alpha \in \mathcal{V}_{\theta\alpha} \\ \int_A \left(-\delta\theta_{(\alpha,\beta)} m_{\alpha,\beta} + q_\alpha \delta\gamma_\alpha\right) = \int_A (\delta_w F - \delta\theta_\alpha C_\alpha) - \\ \int_{\Gamma_M} \delta\theta_\alpha M_\alpha + \int_{\Gamma_Q} \delta_w Q \qquad \forall x \in A \end{cases}$$

Where M_α and Q are the prescribed moments and shear forces (natural or Neumann boundary conditions) Γ_M and Γ_Q are the Neumann frontiers.

From the variational formulation and discretizing the **Ω** domain, the finite element formulation is determined:

$$(L^{FEM})\begin{cases} Considering\ \mathbf{K} \in \mathbb{R}^{NxN}\ and\ \mathbf{F} \in \mathbb{R}^M, \\ find\ \mathbf{d}\ such\ that: \\ \mathbf{K}\,\mathbf{d} = \mathbf{F} \end{cases}$$

Where **d** is the nodal displacement value $\mathbf{d} = \begin{bmatrix} w \\ \theta_1 \\ \theta_2 \end{bmatrix}$

Where:

$$K_{ij} = \iint_A B_i^T \hat{D} B_j \, dA \ ;$$

$$F = \iint_A N^T p_j - \int_{\Gamma_M} N^T \overline{M} + \int_{\Gamma_Q} N^T \overline{Q}$$

$$p_j = [f_z \quad m_x \quad m_y]^T$$

$\hat{D}$ is the generalized constitutive matrix.

The stiffness matrix of each element can be divided into bending (k_b) and transverse shear (k_s). The global equilibrium equation is written as

$$(K_b + K_s)d = F \qquad (1)$$

$$K_{ij}^{(e)} = \iint_{A^{(e)}} \begin{bmatrix} B_{bi}^T & B_{si}^T \end{bmatrix}^T \hat{D} \begin{bmatrix} B_{bj} \\ B_{sj} \end{bmatrix} dA = K_{b_{ij}}^{(e)} + K_{s_{ij}}^{(e)} \qquad (2)$$

Where:

$$B_{bi} = \begin{bmatrix} 0 & N_{i,x} & 0 \\ 0 & 0 & N_{i,y} \\ 0 & N_{i,y} & N_{i,x} \end{bmatrix}; \quad B_{si} = \begin{bmatrix} N_{i,x} & -N_i & 0 \\ N_{i,y} & 0 & -N_i \end{bmatrix}$$

The vector of forces remains:

$$F^{(e)} = \iint_{A^{(e)}} N^{(e)T} p_j - \int_{\Gamma_M^{(e)}} N^{(e)T} \overline{M} + \int_{\Gamma_{Q^{(e)}}} N^{(e)T} \overline{Q}^{(e)} \qquad (3)$$

Where:

$$N_i = \begin{bmatrix} N_i & 0 & 0 \\ 0 & N_i & 0 \\ 0 & 0 & N_i \end{bmatrix}$$

2.3 TYPE OF ELEMENTS CONSIDERED

In order to verify the accuracy of the model, four different elements were implemented: Q4, QS8, QL9, and QH9 based on [9]. The shape functions referring to these elements are presented below:

- Four-node element – Q4

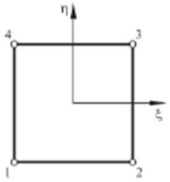

Figure 2: *Bilinear element (Q4).[9]*

$$N_i = \frac{1}{4}(1 + \xi\xi_i)(1 + \eta\eta_i), i = 1,2,3,4 \qquad (4)$$

- Eight-nodes element – QS8

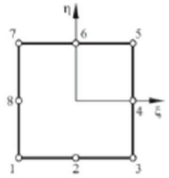

Figure 3: *Serendipity Quadratic element (QS8).[9]*

$$N_i = \frac{1}{4}(1+\xi\xi_i)(1+\eta\eta_i)(\xi\xi_i+\eta\eta_i-1), i = 1,2,3,4$$
$$N_i = \frac{1}{2}(1+\eta\eta_i)(1-\xi^2), i = 5,7 \quad (5)$$
$$N_i = \frac{1}{2}(1+\xi\xi_i)(1-\eta^2), i = 6,8$$

- Nine-nodes element – QL9

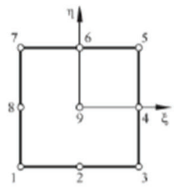

Figure 4: *Lagrangian Biquadratic element (QL9).[9]*

$$N_i = \frac{1}{4}(\xi^2+\xi\xi_i)(\eta^2+\eta\eta_i), i = 1,3,5,7$$
$$N_i = \frac{1}{2}\eta_i^2(\eta^2+\eta\eta_i)(1-\xi^2)+\frac{1}{2}\xi_i^2(\xi^2+\xi\xi_i)(1-\eta^2)$$
$$, i = 2,4,6,8$$
$$N_i = (1-\xi^2)(1-\eta^2), i = 9 \quad (6)$$

- Nine-nodes hierarchical – QH9

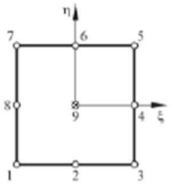

Figure 5: *Hierarchical element (QH9).[9]*

$$\theta_x = \sum_{i=1}^{8} N_i\,\theta_{x_i} \;;\; \theta_y = \sum_{i=1}^{8} N_i\,\theta_{y_i}$$
$$w = \left(\sum_{i=1}^{8} N_i w_i\right) + \overline{N_9} w_9 \quad (7)$$

where N_i are the standard shape functions for the QS8 element and $\overline{N_9} = (1-\xi^2)(1-\eta^2)$. The hierarchical variable w_9 is the difference between the nodal deflections obtained with QS8 and QL9 elements. [9]

2.4 DETERMINATION OF THE BEST ELEMENT TO BE USED

The performance and meshing of the implemented plates with different elements were compared against the analytical solutions from the author S. Timoshenko [12], through the results of the vertical displacement in the center of the plate.

In Figure 6, it shows that the four elements give a result like to Timoshenko formulation due to the low percentage error (i.e., less than 5%) in vertical displacement, however, the QH9 element shows the best accuracy (i.e., 0.002%) due to the addition of a "spring" that eliminates spurious mechanisms [9]. The next steps of this investigation were carried out with the QH9 element.

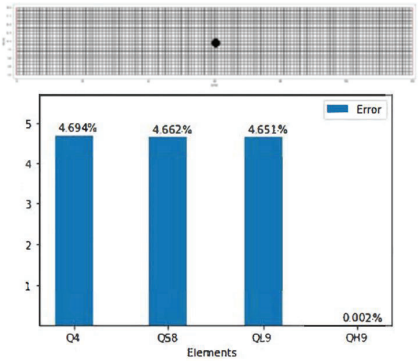

Figure 6: *(up) Evaluation in the center of the discretized plate, (down) Graph of the percentage error of each element.*

3 EVALUATION OF NATURAL DEFECTS ON WOOD PLATES

In each computational model, the displacement and deformation fields were calculated. Subsequently, to evaluate the behavior of the plate, the knotty areas were used, taking as a reference the properties of the Blass study [3], in addition, the properties and distribution of the knotty areas in Radiata Pine specie were replicated. The Knotty Area Ratio (KAR) is varied increasing from 0.1 to 1 to evaluate the impact on the displacement and stress in three control points along the simulated plate (P1, P2, and P3 illustrated in Figure 8). The coordinates of each point are located at (Lx/4, Ly/2), (Lx/2, Ly/2), (3Lx/4, Ly/2) respectively. To evaluate the stress interaction in the plate, the Von Misses Normalized [14] and Tsai-Wu [13] failure criteria were used.

In order to evaluate the effect of knotty area distribution, five hundred wood plates with a fixed KAR but with a different distribution of knotty areas, varying the whorl of internodes and whorls were assessed. The center point of the plate is chosen as the control point and the vertical displacement of the 500 wooden plates is plotted.

3.1 EFFECT OF THE KNOTTY AREA

In order to quantify the accuracy of the model, a virtual test of a representative 120 cm x 20 cm x 6.5cm wood plate made of Radiata Pine grown in Chile was simulated (see Figure 7). A rectangular orthotropic law was considered for the wood constitutive, considering the

https://doi.org/10.52202/069179-0052

mechanical properties from [4]. The model was considered as simply supported and uniformly loaded with 4 [N/cm^2] over the entire surface. The geometry of the element was discretized into 1 cm x 1 cm elements. To include the effect of the knotty area in the model, discrete length stripes were considered whose properties were calculated by means of a linear regression equation determined experimentally in reference [3] based on the knotty area ratio (KAR) (see eq. 8 and 9). The dimensions of the knotty areas (whorl and internode length, see Figure 8) were determined from a study on Radiata Pine grown in Chile (see Table 1) [8].

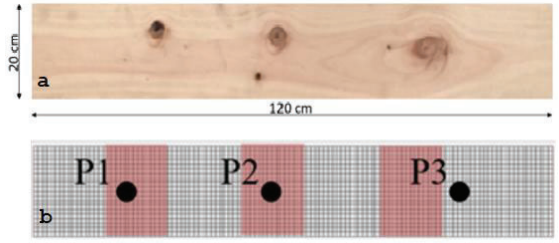

Figure 7: *(a) Representative timber element, (b) Discretization of the wooden plate with the knotty area.*

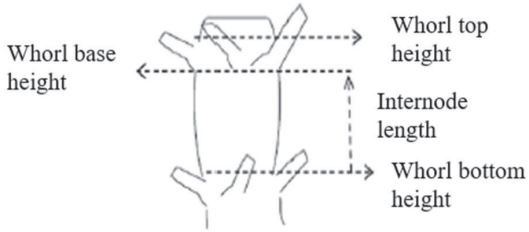

Figure 8: *Base height and top of a whorl. Taken from [8]*

Table 1: *Branch range of the Radiata Pine tree in regions VII and IX of Chile. Take from [8].*

Variable	Range
Internode length [cm]	30 - 110
Whorl length [cm]	20 - 40

$$\ln(\mathrm{E_L}) = 7.90 + 3.81 * 10^{-3} * \rho_0 - 0.369 * KAR$$

With r = 0.773 and S_R = 0.165 (8)

$$\ln(f_\mathrm{L}) = -9.09 + 1.36 * ln(\mathrm{E_L}) - 0.978 * KAR$$

With r = 0.839 and S_R = 0.274 (9)

Where the modulus of elasticity (E_L), resistant tension in flexion (f_L) are in N/mm^2, anhydrous density (ρ_0) in kg/m^3 and the KAR is dimensionless.

3.2 EFFECT OF THE WHORL AND INTERNODE LENGTH

In order to understand the behavior of the timber elements with knotty areas of different lengths of internodes and whorls, a fixed KAR of 66% (KAR = 0.66) was considered to simulate 500 cases with different knotty area dimensions (i.e., whorl and internode length variation) through the Monte-Carlo method.

3.3 FAILURE CRITERIA

3.3.1 VON MISES NORMALIZED

In the reference [14] the authors develop a simplified method for the evaluation of the failure by the resistant tension in flexion (f_L).

$$\frac{\sigma_{vm}}{f_L} = \frac{\sqrt{\sigma_{xx}^2 - \sigma_{xx}\sigma_{yy} + \sigma_{yy}^2 + 3\tau_{xy}^2}}{f_L} \leq 1 \quad (10)$$

Where: σ_{xx}, σ_{yy}, τ_{xy}, are the uniaxial and shearing stress components in the respective directions and sections of an isotropic model and f_L is given by equation 8.

3.3.2 TSAI-WU

For a planar orthotropic model, the failure criteria is given by:

$$F_1\sigma_L + F_2(\sigma_R + \sigma_T) + F_{11}\sigma_L^2 + F_{22}(\sigma_R^2 + \sigma_T^2 + 2\tau_{RT}^2) + F_{66}(\tau_{LR}^2 + \tau_{LT}^2) + 2F_{12}(\sigma_L\sigma_R + \sigma_L\sigma_T) + 2F_{23}(\tau_{RT}^2 - \sigma_R\sigma_T) \leq 1 \quad (11)$$

Where: σ_L, σ_R, σ_T, τ_{LR}, τ_{RT}, τ_{LT} are the uniaxial and shearing stress components in the respective directions and sections of an orthotropic model. F_1, F_2, F_{11}, F_{22}, F_{66} and F_{23} are coefficients obtained from uniaxial stresses (i.e., in tension f_t and compression f_c) and shear stress f_v parallel or perpendicular to the grain (i.e., denoted as 0 or 90 for parallel or perpendicular, respectively), through the reference [7]. F_{12} is a coefficient that represents, the biaxial resistance (parallel and perpendicular).

$$F_1 = \frac{1}{f_{t0}} - \frac{1}{f_{c0}};\ F_2 = \frac{1}{f_{t90}} - \frac{1}{f_{c90}}$$

$$F_{11} = \frac{1}{f_{t0}f_{c0}};\quad F_{22} = \frac{1}{f_{t90}f_{c90}}$$

$$F_{66} = \frac{1}{(0.72f_{v0})^2};\quad F_{23} = \frac{1}{2}\left(\frac{1}{f_{v90}^2} - \frac{1}{f_{t90}f_{c90}}\right)$$

For the factor F_{12} the reference [6] proposes the following:

$$F_{12} = \frac{1}{2}\left(\frac{1}{f_{t0}f_{c90}} + \frac{1}{f_{c0}f_{t90}} - \frac{1}{f_{v0}^2}\right)$$

Experimental data from reference [10] in Radiata Pine is taken into consideration for defining the uniaxial and

shear stress input necessary for calculating the coefficients, F_i. The characteristics will be considered in a dry condition (humidity < 19%).

4 RESULTS

The results of the computational plate model based on QH9 elements are illustrated in Figures 9 to 11, where the displacements and stresses variation as a function of the knotty area ratio (KAR), whorl length, and internode length are evaluated.

4.1 DISPLACEMENT AND DEFORMATION FIELD

The displacements and stresses of the plate are shown in Figure 9 considering a plate without a knotty zone and another with a KAR of 66%. Figure 9.a shows that the vertical displacement at the edge of the plate increases by 12% because of the knotty area effect. Figure 10 shows visually how the KAR influences the stress distribution.

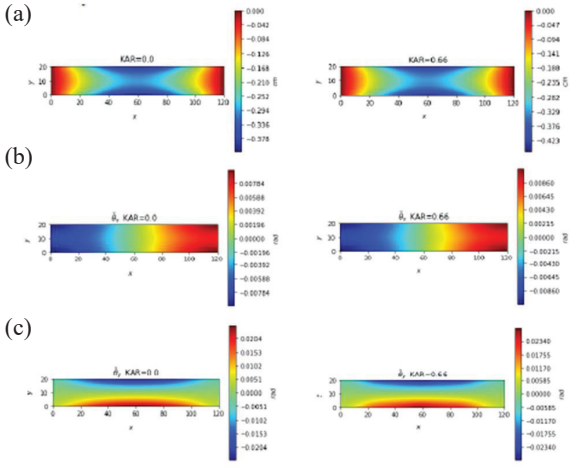

Figure 9: *(left) KAR=0.0, (right) KAR=0.66. (a) Vertical displacement, (b) rotation about X-direction and (c) rotation about Y-direction*

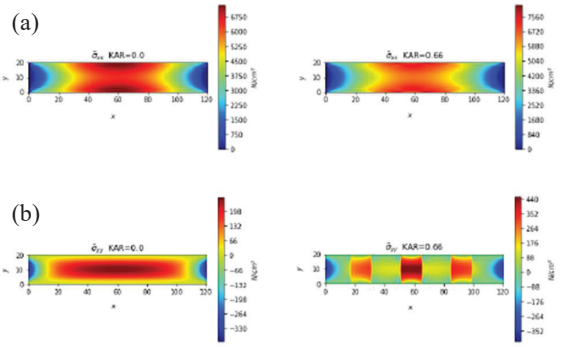

Figure 10: *(left) KAR=0.0, (right) KAR=0.66. Stress field in (a) X and (b) Y direction, respectively*

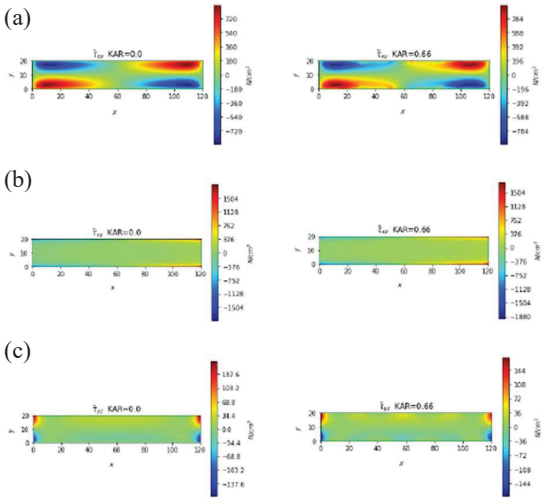

Figure 11: *(left) KAR=0.0, (right) KAR=0.66. Shear stress field (a) XY, (b) XZ and (c) YZ.*

4.2 FAILURE CRITERIA

Two failure criteria were selected to analyze the stress state in the evaluated wood plate. By using the Tsai-Wu criterion, the area where the failure is expected to occur can be identified due to the integration of all the stresses that interact in the plate and the consideration of real Radiata Pine wood coefficients F_i. On the other hand, the Von Mises Normalized criterion does not consider stresses interaction since it is designed for isotropic materials.

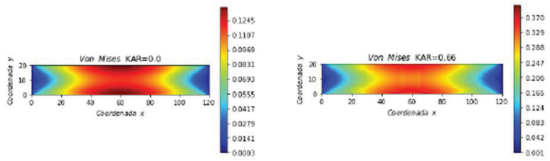

Figure 12: *Failure criterion Von Mises Normalized with (left) KAR=0.0 and (right) KAR=0.66.*

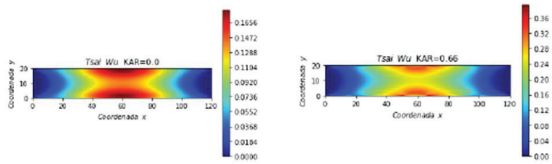

Figure 13: *Failure criterion Tsai Wu with (left) KAR=0.0 and (right) KAR=0.66.*

4.3 EFFECT OF THE KNOTTY AREA

Considering out-of-plane displacement results (see Figure 14), it is observed that as the KAR increases, the vertical displacement increases proportionally, generating an increase of up to 19% in the out-of-plane displacement, being the point P2 with the highest displacement increments, the rotation θ_x increases by 14% at points P1 and P3.

https://doi.org/10.52202/069179-0052

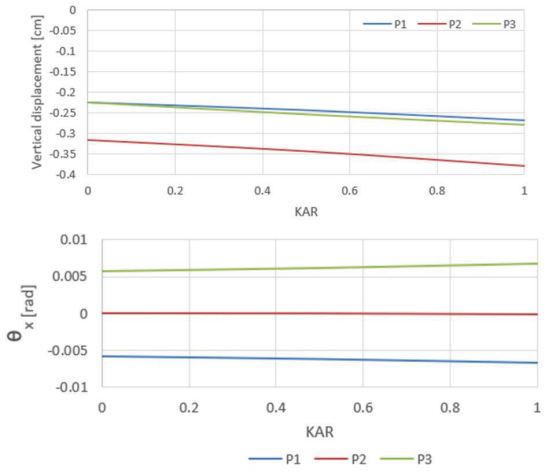

Figure 14: *Effect of the KAR in (top) vertical displacement and (bottom) rotation about X.*

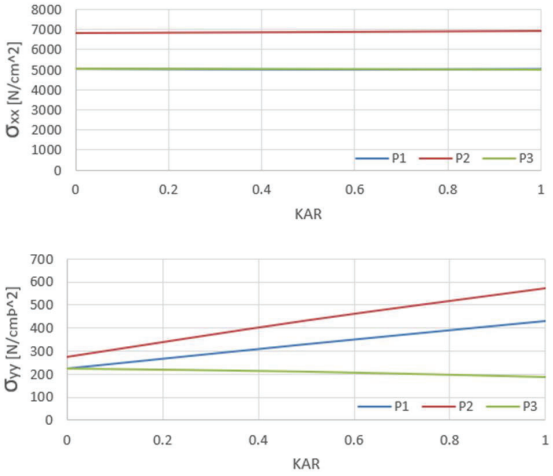

Figure 15: *Effect of the KAR in (top) stress xx and (bottom) stress yy.*

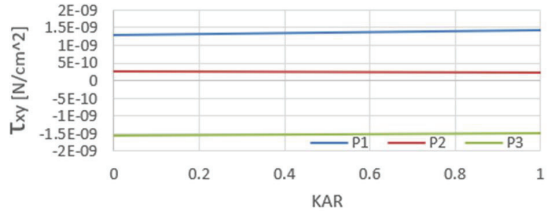

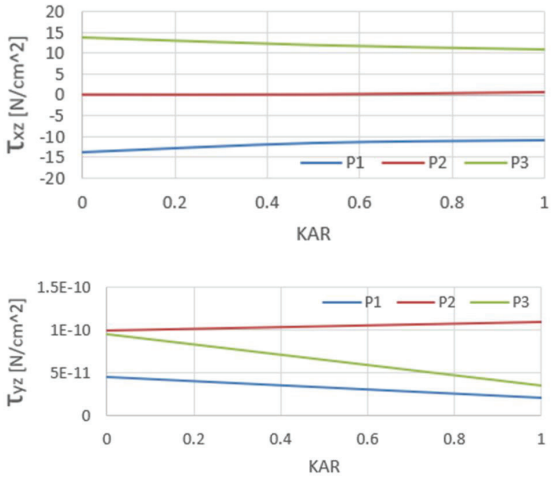

Figure 16: *Effect of the KAR in (top) Taú xy, (middle) Taú xz and (bottom) Taú yz.*

Figure 15 shows that as the KAR increases, the stresses yy (σ_{yy}) increase proportionally, causing a high stress concentration at the points with knotty areas.

Figure 17 shows that for KAR values less than 0.5, the Tsai-Wu criterion is the most conservative in predicting failure whereas for KAR values greater than 0.5 the Von Mises Normalized criterion is the most conservative for failure prediction. The Tsai-Wu criterion utilization factor shows an increment of up to 56% as the KAR increases, while the Von Mises Normalized criterion produces an increment of up to 78%.

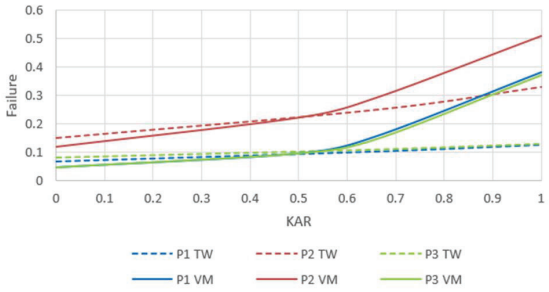

Figure 17: *Effect of the KAR in failure criteria utilization factor.*

4.4 EFFECT OF THE WHORL AND INTERNODE LENGTH

Figure 18 illustrates the evolution of the vertical displacement (*D*) for the 500 simulated cases measured in point P2, considering a KAR=0.66 and varying the lengths of internodes and whorls. Moreover, there is a minimum of one knotty area along the length. From the simulation results, equation 12 is proposed by using the least squares method.

https://doi.org/10.52202/069179-0052

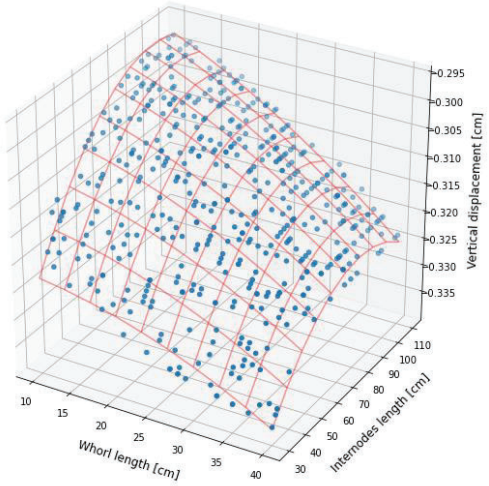

Figure 18: *Vertical displacement at node P2 of the 500 simulated wooden plates with KAR=0.66.*

$$D = 1.879 \cdot 10^{-4} \cdot W + 1.178 \cdot 10^{-3} \cdot I - 1.034 \cdot 10^{-5} \cdot W^2 - 5.256 \cdot 10^{-6} \cdot W \cdot I - 5.803 \cdot 10^{-6} \cdot I^2 \quad (12)$$

Where D= vertical displacement [cm], W= whorl length [cm] and I= internode length [cm].

Figures 19 and 20 show an increment of up to 14% in the vertical displacement depending on internode length or whorl length.

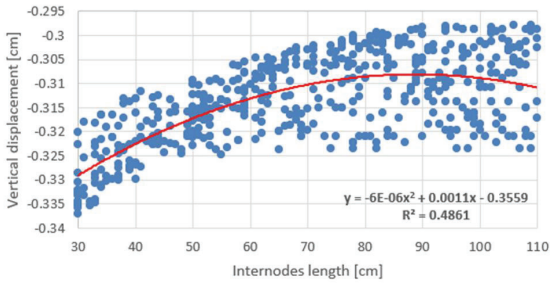

Figure 19: *Vertical displacement v/s internodes length.*

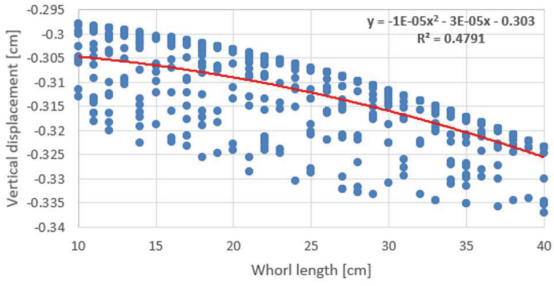

Figure 20: *Vertical displacement v/s whorl length.*

The contour plot shows that the longer the internode length and the shorter the whorl length, the smaller the vertical displacement. On the other hand, between shorter internodes length and greater whorl lengths, the vertical displacement is greater. In the first case, since the length of the internode is so large, it only reaches to one knotty zone along the plate length while the shorter the internode is, there are more knotty zones along the plate. Due to the dimensions of the plates, it only reaches a maximum of three knotty areas.

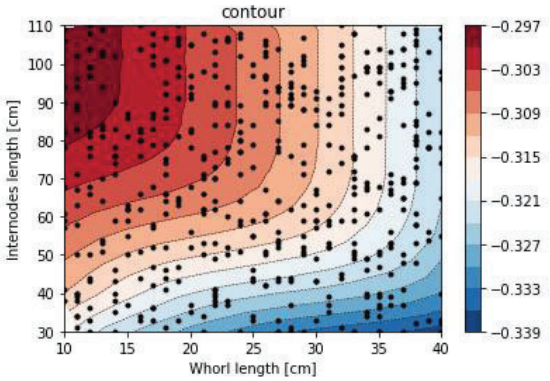

Figure 21: *Internodes length v/s whorl length effect on the vertical displacement at node P2.*

5 CONCLUSIONS

The Python-based model was able to capture the effect of the knotty areas in the response of wood plates subjected to out-of-plane bending. When the KAR reaches its maximum value, the stiffness and strength of the plate decrease by 19% and 56%, respectively. The previous statement can be supported by the failure criteria which takes its maximum values in the wood adjacent to the knotty areas in the center of the plate. Talking about the effect of different lengths of internodes and whorls, the shorter the length of the internode and the longer the whorl, the greater the vertical displacement of the plate, reaching an increment of up to 14%. It is concluded that the open-source numerical model was able to capture the effect of the knotty areas on the bending behavior of timber elements. The next step involves the calibration of the input parameters of the numerical model from the test results.

REFERENCES

[1] Aguilera Fernández, M., Benedetti Ruiz, S., Gallardo Lara, C., & Ulloa, D. *Estudio percepción construcción en madera.* 2020

[2] Cook, R.D., Malkus, D.S., Plesha, M.E., & Witt, R.J.: *Concepts and Applications of Finite Element Analysis.* Fourth edition John Willey and Sons, 2002.

[3] Flaig, M. Blass, H.J.: *Bending strength of cross laminated timber beams loaded in plane.* Proceedings of WCTE 2014, 2014.

[4] Guindos, P.: *Fundamentos del diseño y la construcción con madera. Primera Edición*, 2019.

https://doi.org/10.52202/069179-0052

[5] Hughes, T. J. *The finite element method: linear static and dynamic finite element analysis.* Courier Corporation. 2012
[6] Liu, J. Y. *Evaluation of the tensor polynomial strength theory for wood*. Journal of Composite Materials, 18(3), 216-226. 1984
[7] Mascia, N. T., Nicolas, E. A., Cammpinas, S., & Todeschini, B. R. *Comparison between Tsai-Wu failure criterion and Hankinson's formula for tension in wood.* Wood Research, 56(4), 499-510. 2011
[8] Millar Ortiz, J.A.: *Análisis del crecimiento diametral de ramas de Pinus Radiata D. Don en distintos sitios entre las Regiones VII y IX*, 2003.
[9] Oñate, E.: *Structural analysis with the finite element method. Linear statics: volume 2: beams, plates and shells.* Springer Science & Business Media, 2013.
[10] Perez, V. *Comprendio de Directrices para enseñanza en ingeniería*. CORMA. 2003
[11] Spiess, A. N., & Neumeyer, N. (2010). An evaluation of R 2 as an inadequate measure for nonlinear models in pharmacological and biochemical research: a Monte Carlo approach. BMC pharmacology, 10(1), 1-11.
[12] Timoshenko, S., & Woinowsky-Krieger, S.: *Teoría de placas y láminas.* Urmo, 1970.
[13] Tsai, S. W., & Wu, E. M. *A general theory of strength for anisotropic materials*. Journal of composite materials, 5(1), 58-80. 1971
[14] Valdivieso D., & Vargas L. *Simulación Númerica del Efecto de los nudos en el Estado Tensional de Placa de Pino Radiata Sometida a Flexión*. 2019.
[15] Zienkiewicz, O.C., Taylor, R.L., J.Z. Zhu.: *The finite element method. Volume 2: Solid Mechanics*. Fifth edition, Butterworth-Heinemann, 2000.